



LAWRENCE
LIVERMORE
NATIONAL
LABORATORY

Dynamics and power balance of near unity target gain inertial confinement fusion implosions

A. Pak, L. Divol, D. T. Casey, S. F. Khan, A. L. Kritcher, J. E. Ralph, R. Tommasini, C. Trosseille, A. B. Zylstra, K. L. Baker, N. W. Birge, R. Bionta, B. Bachmann, E. L. Dewald, T. Doeppner, M. S. Freeman, D. N. Fittinghoff, V. Geppert-Kleinrath, H. Geppert-Kleinrath, K. D. Hahn, M. Hohenberger, J. Holder, S. Kerr, Y. Kim, B. Koziowski, K. Lamb, B. J. MacGowan, A. G. MacPhee, K. D. Meaney, A. S. Moore, D. J. Schlossberg, S. Stoupin, P. Volegov, C. Wilde, C. V. Young, O. L. Landen, R. P. J. Town

March 14, 2023

Physical Review Letters

Disclaimer

This document was prepared as an account of work sponsored by an agency of the United States government. Neither the United States government nor Lawrence Livermore National Security, LLC, nor any of their employees makes any warranty, expressed or implied, or assumes any legal liability or responsibility for the accuracy, completeness, or usefulness of any information, apparatus, product, or process disclosed, or represents that its use would not infringe privately owned rights. Reference herein to any specific commercial product, process, or service by trade name, trademark, manufacturer, or otherwise does not necessarily constitute or imply its endorsement, recommendation, or favoring by the United States government or Lawrence Livermore National Security, LLC. The views and opinions of authors expressed herein do not necessarily state or reflect those of the United States government or Lawrence Livermore National Security, LLC, and shall not be used for advertising or product endorsement purposes.

Dynamics and power balance of near unity target gain inertial confinement fusion implosions

A. Pak,¹ L. Divol,¹ D. T. Casey,¹ S. F. Khan,¹ A. L. Kritcher,¹ J. E. Ralph,¹ R. Tommasini,¹ C. Trosseille,¹ A. B. Zylstra,¹ K. L. Baker,¹ N. W. Birge,² R. Bionta,¹ B. Bachmann,¹ E. L. Dewald,¹ T. Doeppner,¹ M. S. Freeman,² D. N. Fittinghoff,¹ V. Geppert-Kleinrath,² H. Geppert-Kleinrath,² K. D. Hahn,¹ M. Hohenberger,¹ J. Holder,¹ S. Kerr,¹ Y. Kim,² B. Kozioziemski,¹ K. Lamb,² B. J. MacGowan,¹ A. G. MacPhee,¹ K. D. Meaney,² A. S. Moore,¹ D. J. Schlossberg,¹ S. Stoupin,¹ P. Volegov,² C. Wilde,² C. V. Young,¹ O. L. Landen,¹ and R. P. J. Town¹

¹*Lawrence Livermore National Laboratory, Livermore, California, 94550, USA*

²*Los Alamos National Laboratory, Los Alamos, New Mexico, 87545, USA*

(Dated: November 15, 2023)

The change in the power balance, temporal dynamics, emission weighted size, temperature, mass, and areal density of inertially confined fusion plasmas have been quantified for experiments that reach target gains up to 0.72. It is observed that as the target gain rises, increased rates of self-heating initially overcome expansion power losses. This leads to reacting plasmas that reach peak fusion production at later times with increased size, temperature, mass and with lower emission weighted areal densities. Analytic models are consistent with the observations and inferences for how these quantities evolve as the rate of fusion self-heating, fusion yield, and target gain increase. At peak fusion production, it is found that as temperatures and target gains rise, the expansion power loss increases to a near constant ratio of the fusion self-heating power. This is consistent with models that indicate that the expansion losses dominate the dynamics in this regime.

Creating a controlled fusion reaction that produces more energy than supplied to initiate it (i.e. target gain > 1) is a grand scientific challenge with broad societal implications[1, 2]. An outstanding issue for each approach pursuing this goal is creating plasma conditions in which Lawson’s criteria[3], where the power of fusion self-heating exceeds all the power losses of the system, is satisfied. Recently, the first inertial confinement fusion (ICF) experiment to satisfy the Lawson Criteria was performed, achieving a target gain of 0.72[4–6]. In the inertial confinement approach, a capsule target containing deuterium and tritium (DT) fuel is imploded in order to achieve the densities and temperatures required for fusion to occur[7]. The achievable target gain and amount of fusion energy produced is directly related to the dynamics of these systems, particularly that of the competition and power balance between fusion induced self-heating versus radiative and expansion losses. Understanding this balance is of fundamental importance and can inform research directions aimed at achieving still higher target gains that are required to access new and novel regimes of plasma science and to realize many of the potential applications and benefits[8].

In this work, we detail the first dynamic observations of the power balance in inertial confinement fusion experiments. Observations of the time-resolved x-ray emission reveal that, for the first time, the increased rate of alpha particle self-heating leads to an increasing reactivity, even as power is lost from the rapid expansion of the fusion plasma. This dynamic leads to a temporal delay in the peak fusion reaction history and an increase in the size, temperature, and mass of DT plasma with increasing fusion energy production. An analytic model[9]

is found to be consistent with these observations. Additionally, unlike prior work[10], in these experiments, due to the increased levels of alpha heating during the expansion phase, the areal density is observed to decrease by $\sim 25\%$ with the observed $5\times$ increase in fusion yield. The analytic model captures this dynamic and indicates for the highest target gain of 0.72, the areal density from the reacting hot spot is approximately half of that of the confining shell. At this target gain, the mechanical PdV/dt work done by the plasma expansion was inferred to be 1.4 ± 0.2 PW at the time of peak neutron production and the power of alpha particle production was measured to be 2.8 ± 0.3 PW. Measurements indicate that as the target gain exceeds ~ 0.25 , the expansion power loss asymptotes to roughly half of the fusion-self-heating power at peak emission. The analytic model and detailed radiation hydrodynamic calculations are found to be consistent with this observation. This indicates that experiments have transitioned into a regime in which the power loss from expansion dominates over all other losses. The analytic model suggests that modest, 2% increases in the kinetic energy supplied to the implosion can increase the fusion yield by up to $3\times$ and can enable target gains > 1 .

In an ICF produced DT plasma, the power balance can be written as,

$$\frac{1}{(\gamma - 1)} \frac{d}{dt}(PV) = f_\alpha P_\alpha - P_{rad.} - P \frac{dV}{dt} - P_{cond.} \quad (1)$$

here γ is the adiabatic index of the plasma, $f_\alpha P_\alpha = f_\alpha E_\alpha P^2 T^{-2} \langle \sigma v \rangle V / 16$ is the power of the α particle self-heating, with f_α being the fraction of energy deposited within the DT plasma. $P_{rad.} \propto P^2 T^{-3/2} V$ is the Bremsstrahlung radiative power loss. In ICF, the central DT plasma is first heated by the mechanical power,

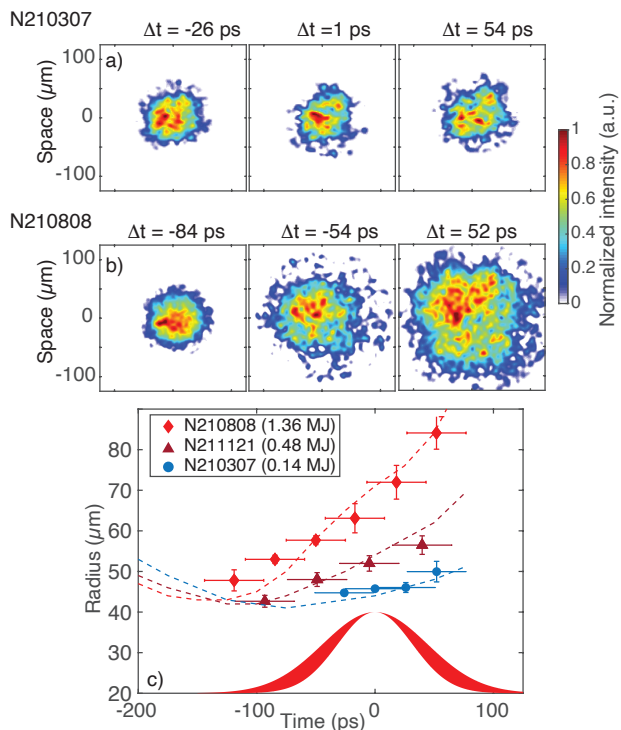


FIG. 1. a-b) Temporally and spatially resolved x-ray emission at photon energies > 10 keV from the reacting hot-spot for two experiments, N210307 and N210808, respectively. For each experiment, the time of each image (Δt) is given with respect to the time of peak x-ray and neutron emission. c) The observed expansion of x-ray emission as a function of time for three experiments and the normalized neutron emission history for N210808 (solid red curve). The dashed lines are model predictions for the x-ray dynamics for implosions that produced 1.36, 0.4, and 0.15 MJ of fusion yield.

PdV/dt , provided by the compressive work done from a spherically imploding shell of DT fuel. After peak compression is reached, the hot spot loses energy and cools by expansion as PdV/dt mechanical work is done on the remaining capsule material. P_{cond} is the power loss associated with thermal conduction and can be neglected as the energy lost from conduction is recycled back into the plasma through mass ablation of the confining DT fuel at the hot spot boundary[11]. In ICF, for ignition to occur, P_α must exceed the sum of all loss terms and have a heating rate that increases faster than the initial increase in the PdV/dt loss rate[10]. Understanding the dynamics and relative balance between heating and loss terms is therefore of critical importance for achieving still higher energy gains.

To understand the dynamics for ICF implosions with target gains of near unity, follow on repeat experiments to the first to satisfy the Lawson Criteria[4] were performed. Each repeat experiment was conducted with as close to the same laser and target conditions as possible. However, differences in the laser delivery and target

quality[12] on the four follow on experiments resulted in lower fusion yields and target gains between 0.25 to 0.7 MJ and 0.13 to 0.36, respectively. Variations in fusion yield have been correlated to $\sim \pm 20\%$ with degradations associated with low mode asymmetries and enhanced radiative loss from ablator material that mixes into the reacting hot spot[12–15]. Data from this set, together with data from prior experiments[16] that achieved lower target gains of < 0.1 , allows for a detailed understanding of how the power balance and associated properties of the reacting hot spot change as a function of α particle self-heating, fusion yield, and target gain.

In these experiments, conducted at the National Ignition facility[17], 192 laser beams, at a wavelength of 351 nm, were used to irradiate the inner surface of a gold-lined depleted uranium cylindrical cavity, called a hohlraum. The lasers had a total energy of 1.9 MJ and a combined peak power of 440 TW. This irradiation produces a near black body x-ray flux with a peak temperature of 310 eV that ablates the surface of a spherical capsule target, with an inner radius of 1050 μm , placed at the center of the hohlraum. The capsule is comprised of an 80 μm thick outer high density carbon ablator[18] that surrounds an inner 65 μm thick shell of cryogenic equimolar DT fuel. The outward ablation triggers an inward compression of the capsule target. During compression, the kinetic energy from the shell is transferred to the internal energy of the reacting hot spot, increasing the average plasma temperature to > 4 keV, which initiates the cascade of fusion reactions.

The escaping neutron spectrum and subsequent reactions are measured by a suite of nuclear diagnostics that measure the fusion emission history[19], time of peak emission[20], and the time integrated size of neutron emission[21]. Additionally, from neutron spectrometers[22], inferences of the emission weighted DT ion temperature and the areal density of the hot spot and DT shell are made from the unscattered and down-scattered neutron spectrum, respectively. From these measurements, time integrated emission weighted inferences of the reacting hot spot mass and pressure can be made[23]. The dynamics of the reacting hot spot can be further understood by observing the Bremsstrahlung x-ray emission which is spatially and temporally resolved by pinhole imaging onto an x-ray framing camera[24] with ~ 10 μm and ~ 100 ps resolution, respectively.

Figure 1 details the dynamics of the hot spot expansion as the rate of α particle heating and total fusion yield are increased. As seen in Fig. 1 a) and c), prior experiments, such as N210307 (N yy-mm-dd) which produced 0.14 MJ of fusion yield show little expansion of the hot spot over the fusion emission time history. Here, peak emission is reached within ~ -25 ps of the time at which minimum radius is obtained and the neutron emissivity begins to decrease as the hot spot expands. In contrast, as seen in Fig. 1 b) and c), for N210808

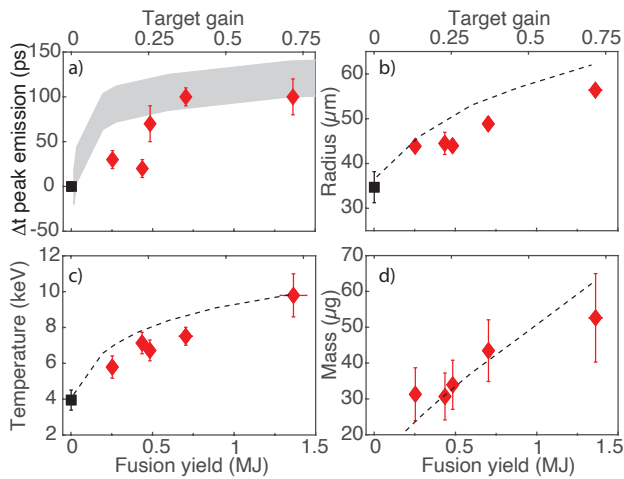


FIG. 2. The change in observed and modeled parameters (shaded and dashed) as a function of yield and target gain. The diamonds and square are for experiments using DT and THD fuel, respectively. a) Delay in peak neutron emission relative to the THD experiment that had a ± 20 ps absolute timing uncertainty which is denoted by the shaded gray band. b) Radius of the time integrated neutron emission. c) Emission weighted neutron temperature. d) Inferred mass of the reacting hot spot.

which produced 1.36 MJ of fusion yield, the hot spot is observed to expand rapidly while the neutron emissivity continues to increase, reaching a maximum ~ 100 ps after the time of minimum radius. As Fig. 1 c) shows, this dynamic is also observed on a follow on repeat experiment N211121 which obtained a fusion yield of 0.48 MJ. The increase in neutron emissivity for N210808 and N211121 as the hot spot rapidly expands is direct evidence that increased levels of α -heating sustains the reactivity, initially overcoming expansion and radiative losses, allowing for increased fusion energy production.

An analytic compressible shell model[9] of these implosions was constructed to gain further insight into the dynamics and compare expectations to observations. Using this model, the temporal and spatial evolution of x-ray emission can be calculated and processed by the instrument response to compare to the observations. The dashed curves in Fig. 1 c) show that these synthetic trajectories capture the relative change in the expansion rate as the overall fusion yield and rate of α -heating are increased. Additional details of this model are given in the supplemental material.

Figure 2 summarizes how the emission history and key hot spot quantities change and evolve as fusion yield is increased. In Fig. 2, the red diamonds are from the set of repeat experiments that used DT fuel while the black square represents a repeat experiment which used a fuel layer of tritium-hydrogen-deuterium (THD) with a molar composition of $\sim 74:25:2\%$. A THD layer was used to reduce the number of DT fusion reactions by $> 1000\times$ and

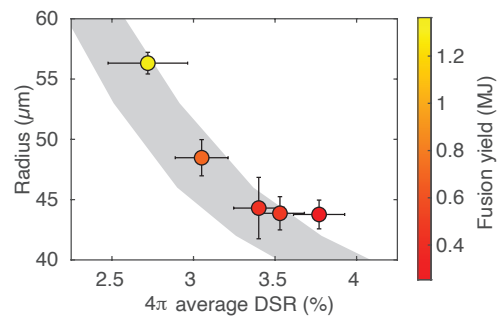


FIG. 3. The observed time integrated neutron emission radius vs. the measured average DSR which reflects areal density of the hot spot and surrounding shell. The gray band is the expected relationship from the compressible shell model with the width set by the range of possible neutron scattering efficiency from DT and remaining carbon.

remove the effects of α -heating on the observed dynamics. In Fig. 2 a), it is observed that as the yield increases, the peak of neutron emission is delayed in time by up to ~ 100 ps. This delay results from the increased rate of α -heating that sustains the reactivity as the hot spot expands, allowing the peak of the neutron emission to be reached at later times, larger radii, and at higher plasma temperatures as seen in Fig. 2 b) and c). This is consistent with the time-resolved x-ray dynamics discussed in Fig. 1. The rise in temperature with fusion yield also increases the ablation rate, which as seen in Fig. 2 d) increases the total amount of mass brought into the hot spot from the higher density confining shell of DT fuel. The shaded band and dashed lines in Fig. 2 show the expected trends of the compressible shell model for these key hot spot quantities. Here, the model input conditions have been held fixed, except for a multiplier on the radiative power loss to approximate the impact of the observed asymmetry and radiative loss degradations. As seen in Fig. 2, this method results in a model that can simultaneously capture the key trends in the hot spot dynamics.

Figure 3 shows that for these experiments, the inferred areal density is observed to decrease by $\sim 25 \pm 5\%$ as the yield increases by $\sim 5\times$. The areal density is inferred using the neutron spectrum with $\rho R_{DT} = C \times DSR$. Here, DSR is the ratio of neutrons down-scattered to 10-12 MeV by the DT plasma and shell to 13-15 MeV component[22] and C is a coefficient associated with the scattering efficiency and hot spot and shell scattering geometry. The decrease in areal density with increasing yield is in contrast to prior work done at lower levels of fusion yields[10] where 30-50% increases in inferred areal density correlated with $\sim 10\times$ increases in fusion yield [23, 25]. This change is associated with the increased levels of α heating and fusion yields causing the majority of neutrons to be produced during the expansion phase where the shell areal density is rapidly decreasing. This

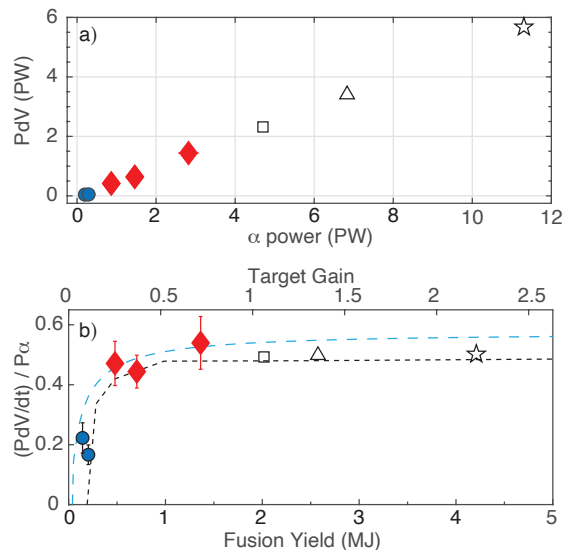


FIG. 4. a) The power of the expanding hot spot (PdV/dt) vs. the fusion α power produced at peak emission for prior experiments and current experiments denoted by the circles and diamonds, respectively. b) The ratio of expansion to alpha power at peak emission vs. fusion yield and target gain. Black dashed curve is expectation from 1D radiation hydrodynamic calculations and the courser blue dashed line represents the analytical expectation. Values predicted by the compressible shell model for design improvements are given by the open symbols.

has been predicted[26] but never before observed. The gray band is the expectation from the compressible shell model and is shown to be in reasonable agreement with observations. The width of the band is associated with the range of C coefficients from 18-19 which are found using dynamic radiation hydrodynamic and static Monte Carlo scattering calculations[27]. In this work, the compressible shell model indicates that with increasing yield, the hot spot areal density increases while the shell areal density decreases. This leads to an increase in the relative contribution from the hot spot to the overall scattering from 11 to 30 %.

The competition between α -heating and hot spot losses that determine the level of fusion yield and target gain can be examined by comparing the rate of fusion heating to expansion losses. Expansion losses are inferred from the temporally and spatially resolved x-ray emission data. Figure 4 a) shows the relationship between the measured PdV/dt expansion power loss versus the self-heating power from α particles at peak emission. Here, the rate of expansion of the x-ray images is used to infer dV/dt and a static hot spot model[23] is used to infer the plasma pressure at peak emission. The compressible shell model suggests that the pressure, P , at peak neutron emission is within $\sim 10\%$ of pressure inferred from the static model. As seen in Fig. 4 a), as the yield and target gain increase, P_α heating and PdV/dt losses

increase by $\sim 14\times$ and $\sim 33\times$ from prior work[16], respectively. To examine how the power balance changes with fusion yield, the ratio between PdV/dt and P_α is shown in Fig. 4 b). It is observed that as the yield and target gain increase, the ratio of $(PdV/dt)/P_\alpha$ first increases as the rate of hot spot expansion increases and then asymptotes to a value of 0.47 ± 0.04 .

This behavior indicates that as the yield and target gain increase, expansion overtakes radiation as the principal power loss mechanism. The asymptotic behavior of $(PdV/dt)/P_\alpha$ can be explained by using the boundary condition that at peak neutron production $dP_\alpha/dt = 0$ and that $\langle\sigma v\rangle T^{-2}$ is constant at this time to rewrite Eqn. 1 as $(PdV/dt)/P_\alpha = \{(\gamma - 1)/(\gamma - 1/2)\}(1 - P_{rad.}/P_\alpha) \approx (4/7)(1 - (4.3/T)^{3.33})$ for $\gamma = 5/3$. Here a temperature power law was used to fit the radiative power loss and the Bosch-Hale reactivity between 5-10 keV. This relationship indicates that as temperature increases, the relative importance of the radiative loss with respect to the α -heating is reduced. The blue dashed curve in Fig. 4 b) shows that this relationship of power balance at peak emissivity is in good agreement with the observed trend. Here the temperature dependence on fusion yield has been fit to the observed trend in Fig. 2 c). To further investigate how the ratio of $(PdV/dt)/P_\alpha$ varies with fusion yield and target gain, a 1D radiation hydrodynamic calculation was first tuned to match the performance of N210808 using the multi-physics code HYDRA[28]. The reactivity was then increased and decreased to study how the ratio of PdV/dt to P_α at peak emission changed with varying yield. The fine black dashed curve in Fig. 4 b) shows that this ratio evolves with increasing fusion yield in a manner consistent to the dynamic seen in the data and expected from analytic estimates.

To explore how the current ICF implosions can be improved to reach higher target gains and fusion yields, the compressible shell model that captures the overall dynamics, key hot spot, and shell quantities is used to explore three different approaches. The open square in Fig. 4 b), is the result of the first approach, which is to conserve the mass of the compressing shell but to increase the in-flight aspect ratio and DT shell density by 2% and 2.8%, respectively. The open triangle and star show the results predicted by the compressible shell model from the second and third approach, which was to increase the overall kinetic energy by 2%, by increasing either the shell mass or shell velocity, respectively. Additional details on the sensitivity of fusion yield to changes in the incident kinetic energy, and how the hot spot quantities evolve at higher yields, are given in the supplemental material. For the increase in shell mass, the width of the shell was increased, while the peak density was held constant. The model indicates that an increased amount of PV work and heating occurs as the return shock transits the additional mass in the thicker shell, leading to an $1.9\times$ increase in fusion yield. Increasing the velocity at

a fixed mass results in an increase in the rate of PdV/dt heating at all times and in fusion yield that is $\sim 2\times$ larger than results from the equivalent increase in kinetic energy using a thicker shell with increased mass. Each approach requires a different laser and target design and some methods may be harder to realize due to increases in instability growth-sensitivity that limit compression or increased asymmetries that reduce coupling. These effects are not considered in the compressible shell model. Nevertheless, this analytic model suggests that modest improvements to the current N210808 design, taken together with mitigations of target defects which lead to variability[12], can result in increased fusion yields and target gains in excess of 1.

In conclusion, this work has detailed for the first time how the observed dynamics and burn averaged plasma conditions of near unity gain inertial confinement fusion implosions change as the amount of fusion self-heating increases. An analytic model is shown to be consistent with the observations and indicates that expansion losses dominate the power balance in this near unity gain regime. The compressible shell model also indicates that higher yields and target gains > 1 can be achieved with modest improvements to the shell compression or kinetic energy. Higher fidelity 2D and 3D radiation hydrodynamic simulations [28, 29] will be used to further investigate the dynamics and guide design changes, seeking to improve fusion yields. This work significantly advances our understanding of power balance in fusion plasmas and provides a framework to future work to study the burn propagation dynamics of ignited plasmas informing what will be required to achieve higher target gains required for many applications.

This work was performed under the auspices of the U.S. Department of Energy (DOE) under Contract No. DE-AC52-07NA27344.

-
- [1] National Research Council, *Burning Plasma: Bringing a Star to Earth* (The National Academies Press, Washington, DC, 2004).
- [2] National Academies of Sciences, Engineering, and Medicine, *Bringing Fusion to the U.S. Grid* (The National Academies Press, Washington, DC, 2021).

- [3] J. D. Lawson, Proceedings of the Physical Society. Section B **70**, 6 (1957).
- [4] H. Abu-Shawareb *et al.* (Indirect Drive ICF Collaboration), Phys. Rev. Lett. **129**, 075001 (2022).
- [5] A. L. Kritcher *et al.*, Phys. Rev. E **106**, 025201 (2022).
- [6] A. B. Zylstra *et al.*, Phys. Rev. E **106**, 025202 (2022).
- [7] J. Lindl, Phys. Plasmas (1994-present) **2**, 3933 (1995).
- [8] National Academies of Sciences, Engineering, and Medicine, *Plasma Science: Enabling Technology, Sustainability, Security, and Exploration* (The National Academies Press, Washington, DC, 2021).
- [9] A. R. Christopherson *et al.*, Physics of Plasmas **25**, 012703 (2018), <https://doi.org/10.1063/1.4991405>.
- [10] P. K. Patel *et al.*, Physics of Plasmas **27**, 050901 (2020), <https://doi.org/10.1063/5.0003298>.
- [11] R. Betti, K. Anderson, V. N. Goncharov, R. L. McCrory, D. D. Meyerhofer, S. Skupsky, and R. P. J. Town, Physics of Plasmas **9**, 2277 (2002).
- [12] L. Divol *et al.*, Physics of Plasmas (to be published).
- [13] A. L. Kritcher *et al.*, Physics of Plasmas **21**, 042708 (2014).
- [14] D. T. Casey *et al.*, Phys. Rev. Lett. **126**, 025002 (2021).
- [15] A. Pak *et al.*, Phys. Rev. Lett. **124**, 145001 (2020).
- [16] A. B. Zylstra *et al.*, Nature **601**, 542 (2022).
- [17] E. I. Moses *et al.*, Fusion Science and Technology **69**, 1 (2016).
- [18] J. Biener *et al.*, Nuclear Fusion **49**, 112001 (2009).
- [19] H. W. Herrmann *et al.*, Review of Scientific Instruments **81**, 10D333 (2010).
- [20] A. S. Moore *et al.*, Review of Scientific Instruments **89**, 10I120 (2018).
- [21] F. E. Merrill *et al.*, Rev. Sci. Instrum. **83**, 10D317 (2012).
- [22] M. G. Johnson *et al.*, Review of Scientific Instruments **83**, 10D308 (2012), <https://doi.org/10.1063/1.4728095>.
- [23] O. A. Hurricane *et al.*, Nature **506**, 343 (2014).
- [24] L. R. Benedetti *et al.*, Review of Scientific Instruments **87**, 023511 (2016).
- [25] S. Le Pape *et al.*, Phys. Rev. Lett. **120**, 245003 (2018).
- [26] J. D. Lindl, S. W. Haan, O. L. Landen, A. R. Christopherson, and R. Betti, Physics of Plasmas **25**, 122704 (2018).
- [27] J. A. Kulesza *et al.*, *MCNP[®] Code Version 6.3.0 Theory & User Manual*, Tech. Rep. LA-UR-22-30006, Rev. 1 (Los Alamos National Laboratory, 2022).
- [28] M. M. Marinak, G. D. Kerbel, N. A. Gentile, O. Jones, D. Munro, S. Pollaine, T. R. Dittrich, and S. W. Haan, Phys. Plasmas **8**, 2275 (2001).
- [29] A. L. Kritcher, R. C. Nora, and C. R. Weber, in preparation (2023).